Universal behavior of the osmotically compressed cell and its analogy to the colloidal glass transition

E. H. Zhou[a], X. Trepat[a,b], C. Y. Park[a], G. Lenormand[a], M. N. Oliver[a], S. M. Mijailovich[a], C. Hardin[c], D. A. Weitz[d], J. P. Butler[a,e], and J. J. Fredberg[a,1]

[a]Program in Molecular and Integrative Physiological Sciences, Harvard School of Public Health, Boston, MA 02115; [c]Division of Pulmonary and Critical Care Medicine, Massachusetts General Hospital, Boston, MA 02114; [d]School of Engineering and Applied Sciences, Harvard University, Cambridge, MA 02138; [e]Department of Medicine, Harvard Medical School, Boston, MA 02115; and [b]University of Barcelona, Institute for Bioengineering of Catalonia and Ciber Enfermedades Respiratorias, 08036 Barcelona, Spain

Edited by Peter G. Wolynes, University of California at San Diego, La Jolla, CA, and approved April 24, 2009 (received for review February 9, 2009)

Mechanical robustness of the cell under different modes of stress and deformation is essential to its survival and function. Under tension, mechanical rigidity is provided by the cytoskeletal network; with increasing stress, this network stiffens, providing increased resistance to deformation. However, a cell must also resist compression, which will inevitably occur whenever cell volume is decreased during such biologically important processes as anhydrobiosis and apoptosis. Under compression, individual filaments can buckle, thereby reducing the stiffness and weakening the cytoskeletal network. However, the intracellular space is crowded with macromolecules and organelles that can resist compression. A simple picture describing their behavior is that of colloidal particles; colloids exhibit a sharp increase in viscosity with increasing volume fraction, ultimately undergoing a glass transition and becoming a solid. We investigate the consequences of these 2 competing effects and show that as a cell is compressed by hyperosmotic stress it becomes progressively more rigid. Although this stiffening behavior depends somewhat on cell type, starting conditions, molecular motors, and cytoskeletal contributions, its dependence on solid volume fraction is exponential in every instance. This universal behavior suggests that compression-induced weakening of the network is overwhelmed by crowding-induced stiffening of the cytoplasm. We also show that compression dramatically slows intracellular relaxation processes. The increase in stiffness, combined with the slowing of relaxation processes, is reminiscent of a glass transition of colloidal suspensions, but only when comprised of deformable particles. Our work provides a means to probe the physical nature of the cytoplasm under compression, and leads to results that are universal across cell type.

compression | cytoplasm | cytoskeleton | mechanotransduction | stiffness

The abilities of the eukaryotic cell to maintain shape, flow, and remodel are mechanical attributes of substantial biological importance (1–5), but our understanding of how cellular constituents give rise to these mechanical attributes remains incomplete. Much of the mechanical rigidity of the cell comes from the cytoskeletal network, composed primarily of actin filaments, microtubules and intermediate filaments. The cytoskeletal network is predominantly under tension; its stiffness increases with tension and thereby increases the forces it can support (6–8). However, filamentous networks typically cannot support appreciable compressive stress because filaments will lose their tension, perhaps even buckle, and thus weaken the network. Nevertheless, cellular compression occurs within tumors (9) and will always occur if the volume of the cell is decreased, as occurs in important physiological processes such as osmotic cell shrinkage, regulatory cell volume decreases (10), preservation of certain animal life forms during drought (anhydrobiosis) (11), and apoptosis (12, 13).

In addition to containing the cytoskeletal network, the intracellular space is filled to near capacity with macromolecules and organelles (14). To describe the mechanical behavior of such a crowded molecular space, a simple approximation might be a colloidal suspension of repulsive particles (15). Indeed, repulsive colloids are known to exhibit sharp increases in shear stiffness as they are compressed and the particle volume fraction increases, ultimately leading to a glass transition in which the colloid transforms from a liquid to a disordered solid (16, 17). Under compression, such an increase in stiffness would compete directly with any weakening of the network. However, the mechanical behavior of the cell upon compression has never been systematically investigated and the consequences of these competing effects remain unknown. Such an investigation is important to determine the role of compression on both the mechanical properties of the cell, and even on the cell volume itself.

In this article, we report the shear stiffness of the living cell subjected to an osmotic compressional stress. As cell volume decreases as a result of water efflux, cell shear stiffness increases with the solid volume fraction in an exponential fashion. Simultaneously, motor-driven relaxation processes persist even at the highest volume fraction but slow by as much as 2 orders of magnitude. These observations suggest that the mechanical properties of a cell under compression are dominated by the contribution of the crowded interior; moreover, they suggest an analogy to a repulsive colloidal suspension approaching its glass transition, but only if the suspension comprises highly deformable particles. Our work provides a framework to characterize the properties of the cell under compression, and enables us to identify behavior that is universal across cell types.

Results

Volume Fraction and Its Dependence on Hyperosmotic Stress. Crowding within the cytoplasm seems to have been sufficiently important in the course of evolution that multiple regulatory mechanisms arose to detect and respond to even small variations of intermolecular spacing (18). In addition to the primary volume response dictated by osmotic equilibrium as governed by van 't Hoff's law, secondary mechanisms of cell volume regulation play out over longer scales of time (10). To perturb cell volume acutely, we subjected the isolated human airway smooth muscle (HASM) cell in culture to sudden hypertonic shock via the addition of 400-Dalton polyethylene glycol (PEG) (*Methods*). Cell volume was measured by atomic force microscopy (AFM) in the adherent cell, and, in separate experiments, by direct

Author contributions: E.H.Z. and J.J.F. designed research; E.H.Z., X.T., C.Y.P., G.L., M.N.O., S.M.M., C.H., and J.P.B. performed research; E.H.Z. and C.Y.P. analyzed data; and E.H.Z., D.A.W., and J.J.F. wrote the paper.

The authors declare no conflict of interest.

This article is a PNAS Direct Submission.

Freely available online through the PNAS open access option.

[1]To whom correspondence should be addressed. E-mail: jeffrey_fredberg@harvard.edu.

This article contains supporting information online at www.pnas.org/cgi/content/full/0901462106/DCSupplemental.

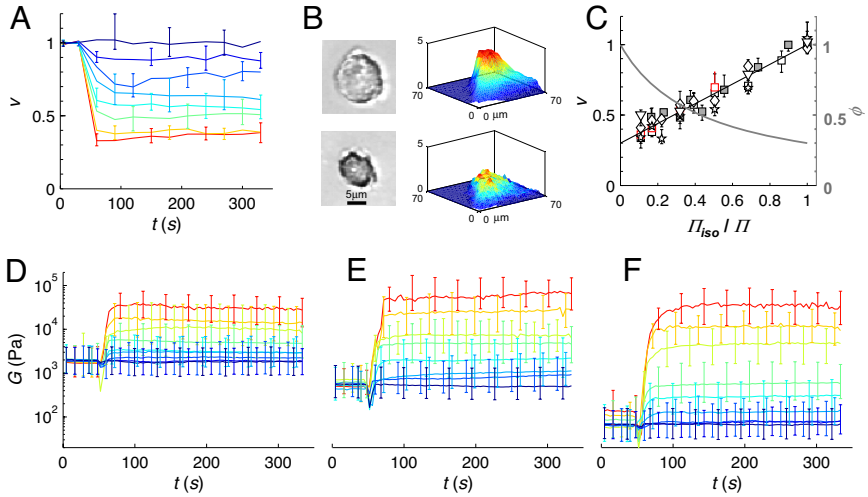

Fig. 1. Hyperosmotic stress decreased the volume and increased the stiffness of HASM cells. (*A*) With the application of hyperosmotic stress at 50 s, cell volume decreased promptly in an osmolality-dependent manner, as measured using optical imaging (*Methods*). $n = 27$ to 73 cells for each dose. The color coding for PEG concentration in *A*, *D*, *E*, and *F* is 0 (darkest blue), 40 (dark blue), 119 (blue), 236 (light blue), 350 (lightest blue), 463 (green), 677 (yellow), 891 (orange), or 1289 (red) mMolal. (*B*) Effect of osmotic stress on cell geometry measured using optical imaging (*Left*) or AFM (*Right*) (*Methods*). Images of the same cells were shown before (*Upper*) and after (*Lower*) applying hyperosmotic stress (1289 mMolal PEG in this example). (*C*) The dependence of relative cell volume on inverse osmotic stress measured using AFM (inverted triangles) or optical imaging (filled squares, open squares, diamonds, stars, and red squares), for different cell types (inverted triangles, open squares, red squares, HASM cells; diamonds, lung fibroblasts; stars, neuroblastoma cells), 2 osmotic agents (filled squares, sucrose; inverted triangles, open squares, diamonds, stars, and red squares, PEG), and actin-depolymerized HASM cells (red squares). $n = 20$ cells for the case measured using AFM; $n = 145$–390 cells for each case tested using optical imaging. In each case, approximately same number of cells was tested for each osmotic stress. (*D–F*) With the application of hyperosmotic stress at 50 s, cell stiffness, monitored with OMTC (*Methods*), increased promptly in an osmolality-dependent manner. Cells with no treatment (*D*), ATP depletion (*E*), or actin depolymerization (*F*), are subjected hyperosmotic medium containing PEG. $n = 2{,}081$–$7{,}663$ beads (≈1 bead per cell) for each treatment. In this and all other figures, a data point with an error bar represents the median value and the interquartile range.

microscopic observation of the suspended cell (Fig. 1*B*) (*Methods*). Over the wide range of osmotic stresses studied, these 2 methods yielded closely similar volume responses (Fig. 1*C*). In response to osmotic shock, cell volume decreased and then equilibrated within a few tens of seconds (Fig. 1*A*) to volumes similar to that of a perfect osmometer (Fig. 1*C*). Similar observations were made for a different osmotic agent (sucrose), after actin depolymerization with latrunculin A, and with 2 different cell types (lung fibroblasts and SY5Y neuroblastoma cells), suggesting that acute changes in cell volume during these extreme challenges was dominated by the primary osmotic response (Fig. 1*C*). Overall, the relationship conformed to the well-known Ponder's relationship (19, 20), $v = R\Pi_{iso}/\Pi + (1 - R)$, with a slope of $R = 0.7$ (black line, Fig. 1*C*), where Π is the applied osmotic pressure, Π_{iso} is the isotonic osmotic pressure, and relative cell volume v is the current cell volume normalized by cell volume under isotonic conditions. Its minimum, v_{min}, occurs at the intercept corresponding to infinite osmotic stress. As such, $v - v_{min}$ is the water volume that is osmotically active, v_{min} is the volume of the cell that is not osmotically active, and the "solid" volume fraction, $\phi = v_{min}/v$, approaches 1 as v approaches v_{min} (gray line in Fig. 1*C*).

With Hyperosmotic Stress, the Cell Shear Stiffness Dramatically Increases. To assess the ability of the cell to resist changes of shape, we used optical magnetic twisting cytometry (OMTC) to probe the force-deformation relationship at 0.75 Hz, from which the complex shear modulus, $G^* = G' + iG''$, can be calculated with the aid of a finite element model (3, 21) (*SI Results and Discussion*). Here, G' and G'' are storage and loss moduli, respectively, and we mainly focus on the magnitude $G = |G^*|$. Cell shear stiffness at isotonic condition, G_{iso}, was stable and close to 2000 Pa. With application of hyperosmotic stress (PEG), cell stiffness increased in a manner that depended on osmolality, consistent with prior reports (22, 23) (Fig. 1*D*). Like the volume response, the stiffening response reached a plateau within a few tens of seconds. As bath osmolality increased and the volume fraction ϕ approached 1 the level of the stiffness plateau dramatically increased (Figs. 1*D* and 2*A*). Extreme osmotic stress caused shear stiffness of the HASM cell to increase by more than an order of magnitude and, as shown below, in other cell types to increase by more than two orders of magnitude. The magnitude of this response can be appreciated by noting that the most extreme challenge with a potent contractile agonist causes the stiffness of these contractile cells, at most, to double (24). Although shear stiffness increased greatly, images of the actin cytoskeleton revealed no remarkable changes (Fig. S1). We further probed the frequency dependence of the cell stiffness. In isotonic steady-state conditions the storage and loss moduli, G' and G'', followed a weak power law over 4 frequency decades (Fig. S2). With progressively increasing osmotic stress, both G' and G'' increased systematically but the power law exponent remained largely constant. Bulk changes of cell volume are described by the osmotic bulk modulus, ϕ ($d\Pi/d\phi$), where Π is the osmotic stress, and it too increased strongly as ϕ approached 1 (*SI Results and Discussion* and Fig. S3).

To assess the generality of these results, we then examined a variety of other cases. When we treated HASM cells with deoxyglucose and sodium azide, which act to deplete adenosine triphosphate (ATP), G_{iso} decreased by over 3-fold (4, 25), but with increasing volume fraction the shear stiffness increased dramatically nonetheless, reaching a value similar to that of the untreated cells (Figs. 1*E* and 2*A*). When we treated these cell with latrunculin A, which acts to depolymerize filamentous actin, G_{iso} decreased by nearly 20-fold but the shear stiffness increased sharply as ϕ approached 1, again reaching a value similar to that of the untreated cells (Figs. 1*F* and 2*A*). When we used a different impermeant solute (sucrose) or a different bead coating (polyL-Lysine, which couples to the cell nonspecifically, as opposed to RGD, which binds to integrins), we found similar

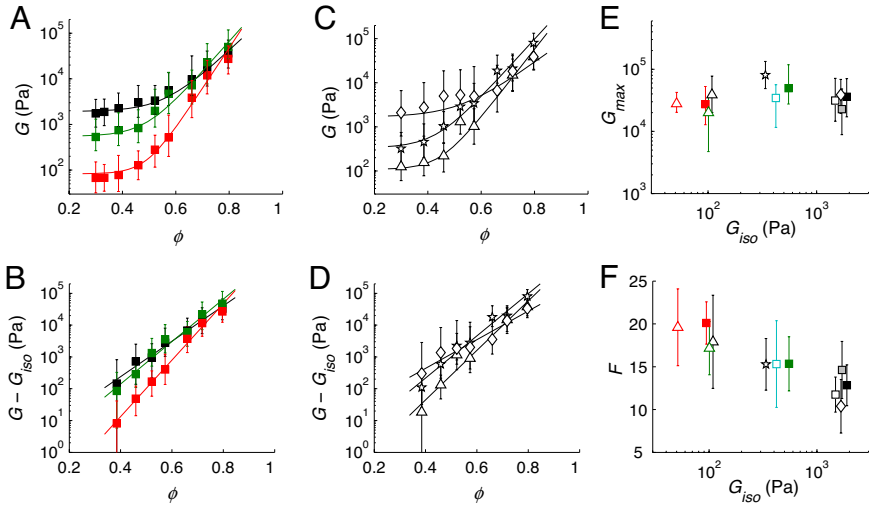

Fig. 2. Dependence of cell stiffness on volume fraction. (*A* and *C*) The relation between stiffness and ϕ for (*A*) HASM cells subjected to no treatment (black), ATP depletion (green) or actin depolymerization using latrunculin A (red), and for (*C*) different cell types with no treatment. In all panels, symbol shape denotes cell type: square, diamond, triangle and star correspond to HASM cells, lung fibroblasts, MDCK cells, and neurons, respectively; different colors stand for different treatments: no treatment (black), ATP depletion (green), cytochalasin D (cyan), and latrunculin A (red). Solid symbols (including filled squares) represent RGD beads; open symbols are PLL beads. PEG was used in all cases, except where sucrose was applied to HASM cells w/o any drug treatment (filled squares). For each case, the sample size is at least 2,000 beads, approximately equally distributed among all doses of osmotic stress. (*B* and *D*) The relative increase in stiffness with respect to the isotonic baseline (G_{iso}) as a function of volume fraction for (*B*) HASM cells with various treatments and for (*D*) different cell types with no treatment. Solid lines represent the relationship $G = G_{iso} + G_o e^{F\phi}$ in *A* and *C*, and $G - G_{iso} = G_o e^{F\phi}$ in *B* and *D*. (*E*) The stiffness at maximum osmotic stress is plotted versus isotonic stiffness for all cases, including different cell types, drug treatments, bead coating and osmotic agents. (*F*) The exponent *F* is plotted versus isotonic cell stiffness. Data points with error bars represent median values and interquartile ranges.

results (see Fig. 2 *E* and *F*). Assuming that the same relationship existed between volume fraction and bath osmolality as in the HASM cell, we then examined 3 other cell types: Madin–Darby canine kidney (MDCK) epithelial cells, SY5Y neuroblastoma cells and human lung fibroblasts. Despite significantly different baseline stiffnesses, in every case the stiffness of these different cell types increased dramatically with increasing volume fraction and appeared to converge at the highest volume fraction (Fig. 2*C*). The maximum value of the stiffness was nearly invariant with G_{iso} and fell in the range of 10^4 to 10^5 Pa (Fig. 2*E*). Accordingly, with changes of cytoskeletal integrity, ATP availability, cell type, solute, or bead coating, the dependence of cell stiffness on volume fraction ϕ was robust and qualitatively similar. Thus, the mechanical properties of the cell under compression are dominated by the contents of the crowded intercellular space, becoming progressively stiffer with increasing osmotic compression.

With Hyperosmotic Stress Spontaneous Nanoscale Motions Dramatically Slow. To gain insights into the intracellular relaxation dynamics, we monitored spontaneous nanoscale motions of a microbead that was tightly coupled to the cytoskeleton (4, 26). When mean square bead displacement (MSD) was resolved as a function of time lag Δt, it exhibited subdiffusive behavior for small Δt and superdiffusive behavior for large Δt (Fig. 3*A*), confirming many previous reports (4, 26, 27). With increasing volume fraction, there was a dramatic reduction in spontaneous bead motions, but even at the maximum volume fraction these motions remained superdiffusive at long time scales indicating persistent nonequilibrium dynamics in the crowded intracellular space (Fig. S4). All these relationships have approximately the same shape and could be scaled onto a single master curve (Fig. 3*A Inset*); as such, this behavior could be fully characterized by the dependence of remodeling dynamics on only one characteristic time. As a measure of this characteristic time, τ, required to achieve a given extent of structural rearrangement, we set an arbitrary threshold value of the MSD (100 nm^2) and then recorded the corresponding time lag needed to achieve that threshold value. As volume fraction increased, τ at first precipitously increased but then reached an approximate plateau (Fig. 3*B*). When ATP was depleted, τ was far larger at baseline, suggesting that baseline rearrangements are actively driven (4), but as volume fraction progressively increased, τ rose to approximately the same plateau value (Fig. 3*B*). F-actin depolymerization by latrunculin A accelerated baseline remodeling by an order of magnitude, but with progressive increase in volume fraction, τ again rose to approximately the same plateau (Fig. 3*B*). Despite such a plateau at high volume fraction, these dynamics depend sensitively on volume fraction near isotonic conditions.

Discussion

With Volumetric Compression, Cell Stiffness Increases in an Exponential Fashion. In isotonic conditions the major determinant of the cellular shear stiffness is known to be the cytoskeletal tensile prestress (6–8, 28), and it is conceivable therefore that increases of G caused by osmotic compression were secondary to underlying increases in this tensile prestress. Much evidence argues against this interpretation, however. Depletion of ATP would be expected to blunt any active contractile response, and, indeed, isotonic stiffness in that case was much smaller but osmotically induced increases in cell stiffness were dramatically enhanced (Fig. 1*D*). Similarly, depolymerization of actin filaments largely ablates cytoskeletal tensile prestress (6), but osmotically induced increases in cell stiffness were seen to be even greater still (Fig. 1*E*). Finally, we measured changes in prestress by studying the isolated airway smooth muscle (ASM) strip (*SI Methods*); for technical reasons, traction force microscopy (6, 7) cannot be used in the context of extreme osmotic stress. When challenged with hyperosmotic stress, the longitudinal stiffness of the ASM strip increased in a manner comparable to the ASM cell in culture, as described above, whereas the prestress did not increase and even tended to decrease (Fig. S5). Taken together, these findings rule out the cytoskeletal network and the tensile

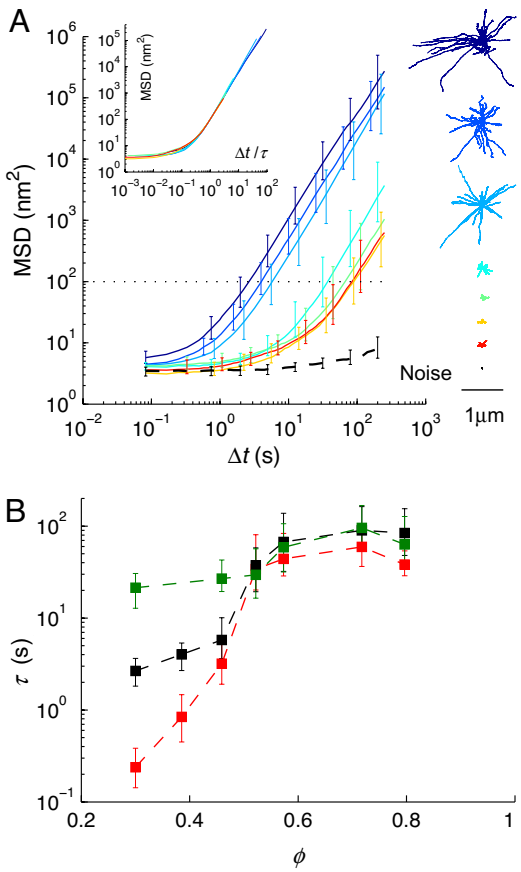

Fig. 3. Hyperosmotic stress suppresses cytoskeleton remodeling in a dose dependent manner. (*A*) MSD of beads tightly bound to cell surface (*Methods*) as a function of time lag for different concentrations of PEG [0 (dark blue), 119 (blue), 236 (light blue), 350 (lightest blue), 463 (green), 891 (orange), and 1289 (red) mMolal] applied to cells originally in isotonic medium. (*Right Insets*) Example trajectories of ≈20 beads over 400 s are shown for each osmotic stress, color code being the same as the main graph. Background measurement noise was quantified using beads fixed on collagen-coated plastic surface by drying (black dash line in the main graph and the black trajectories in *Right Inset*). (*Left Inset*) All MSD curves at different osmotic stress can be collapsed by horizontal shifting. The amount of shift for each curve, τ, is determined by the Δt at which MSD(Δt) crosses 100 nm^2 (the dotted line in the main graph). $n = 136$–201 beads for each dose. (*B*) The dependence of the time scale of remodeling on ϕ is shown for HASM cells treated with ATP depletion (green), latrunculin A (red), or no treatment (black). We quantify the time scale using τ, as defined above in *A*. For each case, the sample size is at least 326 beads, approximately equally distributed among all doses of osmotic stress. Data points with error bars represent median values and interquartile ranges.

prestress that it carries as being responsible for the dramatic rise in cell stiffness as cell volume decreases.

We therefore considered the simplest possible alternative, namely, the notion that the shear stiffness of the cell comprises 2 independent and additive contributions—one attributable to the cytoskeleton network, which is thought to dominate in isotonic conditions (6–8), and the other attributable to the colloidal phase, which becomes increasingly important as water leaves the cell and the volume fraction ϕ increases. If these contributions are additive and independent, then the colloidal contribution would be isolated by subtracting from the measured stiffness (G) of the osmotically compressed cell the isotonic stiffness of that cell (G_{iso}). Upon doing this subtraction, the colloidal contribution is seen to depend on volume fraction exponentially (Figs. 2*B* and 2*D*),

$$G - G_{iso} = G_0 e^{F\phi} \quad [1]$$

where the parameter F quantifies the sensitivity of the colloidal stiffness to changes in volume fraction ϕ, and G_0 represents this stiffness at infinite dilution ($\phi = 0$). The parameter F varied inversely with G_{iso} (Fig. 2*F*) and G_0 varied positively with G_{iso} (Fig. S6). This relationship therefore reveals a simple but universal phenomenological rule by which volumetric compression enhances shear stiffness of the eukaryotic cell.

Under compression, cytoskeletal filaments experience smaller tension, perhaps even buckle, and for either reason will tend to soften. Thus, the relative increase in cell shear stiffness that is observed under osmotic compression cannot be attributed to cytoskeletal network tension and seems to arise mainly from the crowded colloidal cytoplasm. If true, we would expect to see general behavior of cells that remains applicable independent of the state of the cytoskeleton. Indeed, such a behavior is found in Eq. **1**, regardless of the integrity of the cytoskeleton. This provides strong support for a dominant colloidal contribution to the cell's shear stiffness under compressive stress. The approach to the glass transition is exponential in ϕ and data converge at high ϕ in every case, but the sensitivity of stiffness to changes in ϕ differs depending on circumstances (Fig. 2 *B*, *D*, and *F*). For example, the behavior would appear to depend on the relative amounts of polymerized actin, suggesting a potential role of protein shape, and the presence of ATP, indicating that non-equilibrium factors come into play.

Analogy to the Colloidal Glass Transition. This mechanical behavior of the osmotically compressed cell has interesting physical implications. Living cells are under continuous remodeling and relaxation, such as revealed by the spontaneous motions of adherent beads (Fig. 3*A Insets*). These spontaneous motions are consistent with the idea that the cell under isotonic conditions is far from being a simple elastic solid (4). Our data further reveal that even under maximum osmotic compression, relaxation processes persist but become dramatically slowed. Indeed, dramatic slowing of relaxation processes is a hallmark of the glass transition (29). For molecular liquids, decreases in temperature lead to increases in relaxation time until the system becomes frozen into an amorphous solid (29), whereas for colloidal suspensions it is decreases in system volume, and corresponding increases in volume fraction, that lead to such a transition (17). Our MSD data therefore suggest that the behavior of cells under compression is reminiscent of the colloidal glass transition in qualitative terms, but how can we understand osmotically compressed cells in the context of the colloidal glass transition in quantitative terms? Spontaneous bead motions are suggestive, but these motions cannot be used to extract the true relaxation time because they are driven by the motor-generated forces, which are hard to measure and likely to vary with compression.

The relaxation time under a constant external force is thus desirable, and can be quantified via the material viscosity and active rheology. To estimate the cytoplasmic viscosity, η, from the oscillatory shear modulus we used the Cox–Merz rule (30). If $\dot{\gamma}$ is the shear rate in a constant shear experiment, and if ω is the frequency in an oscillatory experiment, then the Cox–Merz rule requires that $\eta|_{\dot{\gamma}=\omega} = G(\omega)/\omega$. It is well established that cell rheology exhibits a weak power law over a wide frequency range (3–5, 8, 25, 31, 32), and that this behavior is explained phenomenologically by the soft glassy rheology (SGR) model (33). This model predicts that for the typical power-law slope (≈0.2) observed in cells (Fig. S2), the Cox–Merz rule will underestimate the viscosity by 40–60% (33). Because this establishes the shear viscosity to well within one order of magnitude, and because the power-law slope is little affected by compression (Fig. S2), this error does not appreciably affect the comparison of viscosities for different compressive stresses. Over a range spanning 4

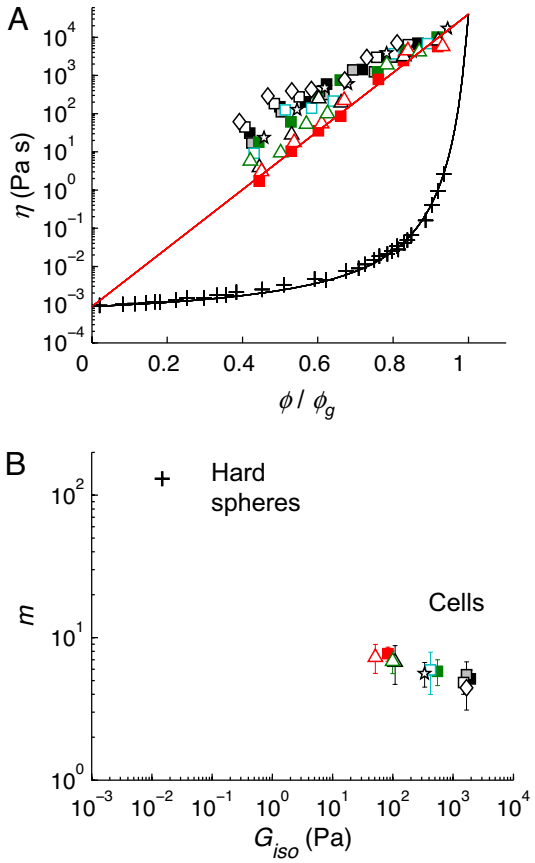

Fig. 4. Cells behave as strong colloidal glass formers. (*A*) Using the Cox–Merz rule, we estimated the viscosity of the colloidal phase of cells (data symbols are the same as used in Fig. 2). The exponential growth of viscosity for cells is sharply contrasted by the stronger increase in viscosity for hard spheres (16), which greatly accelerates as the volume fraction increased toward the glass transition (pluses). In the *x* axis, we normalized the volume fraction by that at the glass transition, defined as the point at which viscosity reaches an arbitrarily chosen high value, 40,000 Pa·s. Data for the hard spheres are fitted with Mooney's equation for hard-sphere viscosity (the black curve), and the red line is the Arrhenius equation with $1/T$ replaced by ϕ. (*B*) We quantified the fragility as $m = d\log_{10}(\eta)/d(\phi/\phi_g)|_{\phi = \phi_g}$, and plotted it against the isotonic stiffness. This stiffness for hard spheres was estimated using the Coz-Merz rule at the volume fraction of 0.3. The fragility of the hard spheres is >1 order of magnitude higher, whereas their ''isotonic stiffness'' is a few orders of magnitude lower, than the corresponding values for cells. Data points with error bars represent median values and interquartile ranges.

decades of viscosity, rheological measurements on osmotically compressed cells therefore suggest that the cytoplasmic viscosity increases exponentially with volume fraction (Fig. 4*A*).

Arrhenius-Like, Strong Glassy Behavior. The exponential manner in which viscosity varies with volume fraction sheds light on the properties of constituent particles and the interactions among them. The viscosity of hard sphere colloids approaching a glass transition varies with volume fraction ϕ as described by Mooney's equation (34), $\eta = \eta_s \exp[\nu\phi/(\phi_0 - \phi)]$, whereas the viscosity of a molecular liquid approaching a glass transition varies with temperature T as described by the Vogel–Fulcher–Tammann (VFT) equation (29), $\eta = \eta_0 \exp[DT_0/(T - T_0)]$. For the former equation, η_s is the solvent viscosity, ϕ_0 is 0.64 for hard spheres, and ν is the crowding factor (1.1 for hard spheres); for the latter, η_0 is the viscosity at infinite temperature, T_0 is the so-called VFT temperature, and D controls the deviation of this relationship from the Arrhenius law. The similarity between these 2 equations suggests that in these systems ϕ and $1/T$ play analogous roles in the approach to the glass transition. We note in particular that in certain limits the Mooney's equation becomes exponential in ϕ, i.e., Arrhenius-like, and fits very well data for cells under compression (Fig. 4*A*). As such, the concept of fragility, which has been instrumental in the categorization of strong versus fragile molecular glass formers (29), can be extended to colloidal glassy systems. We define ϕ_g, the glass transition volume fraction, as the volume fraction at which viscosity reaches an arbitrarily chosen high value, 40,000 Pa·s, and the fragility, m, for the colloidal glass transition as the slope of the relationship between log η versus ϕ/ϕ_g as the latter approaches 1. The fragility for hard spheres is seen to be quite high, whereas the fragility of cells is much lower (Fig. 4*B*). Our data therefore show that the osmotically compressed cell behaves very differently from a suspension of hard spheres; whereas the latter behaves as a fragile glass-former, the eukaryotic cell is reminiscent of a strong glass-former (29).

Physical Basis for Strong Glassy Behavior. That a soft cell under compressive stress behaves as a strong glass is a clear finding and represents the major result of this report. The underlying structures and processes that might account for this finding remain a good deal less clear, however, and represent an open question. We found that ATP depletion strongly modulates the glass transition behavior of the cell, consistent with the notion that nonequilibrium processes may modulate glass transition behavior (35). Similarly, we found that F-actin disruption substantially increases the fragility, consistent with theoretical work demonstrating the effects of particle geometry on glass transition behavior (36). In addition, macromolecules, and organelles within the eukaryotic cytoplasm are far from being compact hard spheres. Even at isotonic volume fraction, it is likely that they interact with each other strongly, unlike the situation for hard sphere suspensions at a similar volume fraction, in which case the particles barely interact. Such interactions potentially explain the much higher viscosity of the cytoplasm compared with that of the hard sphere suspension at the same concentration. More importantly, these ''particles'' are deformable; for example, under the influence of molecular crowding proteins have been shown to deform and change conformation (14, 37). In this respect, then, the cytoplasm resembles a colloidal system of repulsive, deformable particles, exemplified by suspensions of star polymers, block-copolymer micelles, and soft microgel particles. Indeed, these systems often exhibit more gradual increases in viscosity than those found for hard sphere colloids during the approach to glass transition (38, 39). Furthermore, Mattsson et al. demonstrated a direct association between the deformability of individual particles and the fragility characterizing the colloidal glass transition (Mattsson J, Wyss HM, Fernandez-Nieves A, Miyazaki K, Hu Z, Reichman DR, Weitz DA (personal communication) Soft colloids make strong glasses.) Although the mechanistic connection between particle deformability and glass fragility remains unclear (40–42), the strong glassy dynamics of the cytoplasm closely resembles those found in a crowded suspension of repulsive soft colloidal particles (Fig. 4).

In summary, the eukaryotic cell possesses a cytoskeleton that is under tension but also a crowded intracellular space that is under compression. The mechanical behavior of the former is positively determined by tension (6–8) and is reasonably well described by the model for soft glassy rheology (3, 33). By contrast, the behavior of the latter is positively determined by compression and is reminiscent of a suspension of soft, deformable particles capable of undergoing a colloidal glass transition. These findings highlight the rich mechanical behavior of the cell, but also suggest a new mechanism by which the cell could regulate its mechanical behavior.

Methods

We cultured HASM cells, MDCK II cells, SY5Y neuroblastoma cells and human lung fibroblasts (CCL 151) on collagen I-coated 96-well plates (Corning). Hyperosmotic medium was prepared by dissolving PEG or sucrose in isotonic medium. We measured cell volume, using AFM on adherent cells, or optical imaging on trypsinized, rounded cells immobilized onto polyL-Lysine (PLL) (4 kDa) coated plastic well. Using OMTC, stiffness of the cell was measured by actively twisting beads tightly bound to the cell surface (3); dynamic remodeling of the cell was measured by recording the movements of these surface-bound beads in the absence of any active bead twisting (4). The 4.5-μm magnetic beads were coated with either RGD peptides or PLL. We used finite element models to estimate the shear modulus of the cell from OMTC experiments (*SI Results and Discussion*, Figs. S7, S8, and S9). Detailed methods are provided in *SI Methods*.

ACKNOWLEDGMENTS. We thank Michael Wasserman and Emil Millet for technical assistance; Karen Kasza and Dhananjay Tambe for discussions; Reynold Panettieri (University of Pennsylvania Medical Center, Philadelphia), Tao Lu (Harvard Medical School, Boston), Daniel Tschumperlin (Harvard School of Public Health, Boston), and Fei Liu (Harvard School of Public Health, Boston) for providing cells; and Nenad Filipovic, Milos Kojic, and Velibor Isailovic for performing the finite element calculations. This work was supported by grants from National Institutes of Health. The AFM experiments were performed at the Center for Nanoscale Systems (CNS) at Harvard University.

1. Elson EL (1988) Cellular mechanics as an indicator of cytoskeletal structure and function. *Ann Rev Biophys Chem* 17:397–430.
2. Wang N, Butler JP, Ingber DE (1993) Mechanotransduction across the cell surface and through the cytoskeleton. *Science* 260:1124–1127.
3. Fabry B, et al. (2001) Scaling the microrheology of living cells. *Phys Rev Lett* 87:148102.
4. Bursac P, et al. (2005) Cytoskeletal remodelling and slow dynamics in the living cell. *Nat Mater* 4:557–571.
5. Trepat X, et al. (2007) Universal physical responses to stretch in the living cell. *Nature* 447:592–595.
6. Wang N, et al. (2002) Cell prestress. I. Stiffness and prestress are closely associated in adherent contractile cells. *Am J Physiol Cell Physiol* 282:C606–616.
7. Stamenovic D, Suki B, Fabry B, Wang N, Fredberg JJ (2004) Rheology of airway smooth muscle cells is associated with cytoskeletal contractile stress. *J Appl Physiol* 96:1600–1605.
8. Gardel ML, et al. (2006) Prestressed F-actin networks cross-linked by hinged filamins replicate mechanical properties of cells. *Proc Natl Acad Sci USA* 103:1762–1767.
9. Butcher DT, Alliston T, Weaver VM (2009) A tense situation: Forcing tumour progression. *Nat Rev Cancer* 9:108–122.
10. Lang F, et al. (1998) Functional significance of cell volume regulatory mechanisms. *Physiol Rev* 78:247–306.
11. Ricci C, Caprioli M, Fontaneto D, Melone G (2008) Volume and morphology changes of a bdelloid rotifer species (Macrotrachela quadricornifera) during anhydrobiosis. *J Morphol* 269:233–239.
12. Maeno E, Ishizaki Y, Kanaseki T, Hazama A, Okada Y (2000) Normotonic cell shrinkage because of disordered volume regulation is an early prerequisite to apoptosis. *Proc Natl Acad Sci USA* 97:9487–9492.
13. Ernest NJ, Habela CW, Sontheimer H (2008) Cytoplasmic condensation is both necessary and sufficient to induce apoptotic cell death. *J Cell Sci* 121(Pt 3):290–297.
14. Ellis RJ, Minton AP (2003) Cell biology: Join the crowd. *Nature* 425:27–28.
15. Crick FHC, Hughes AFW (1950) The physical properties of cytoplasm. *Exp Cell Res* 1:37–80.
16. Cheng Z, Zhu J, Chaikin PM, Phan SE, Russel WB (2002) Nature of the divergence in low shear viscosity of colloidal hard-sphere dispersions. *Phys Rev* 65(4 Pt 1):041405.
17. Pusey PN, van Megen W (1986) Phase behaviour of concentrated suspensions of nearly hard colloidal spheres. *Nature* 320:340–342.
18. Ellis RJ (2001) Macromolecular crowding: Obvious but underappreciated. *Trends Biochem Sci* 26:597–604.
19. Guilak F, Erickson GR, Ting-Beall HP (2002) The effects of osmotic stress on the viscoelastic and physical properties of articular chondrocytes. *Biophys J* 82:720–727.
20. Ting-Beall HP, Needham D, Hochmuth RM (1993) Volume and osmotic properties of human neutrophils. *Blood* 81:2774–2780.
21. Mijailovich SM, Kojic M, Zivkovic M, Fabry B, Fredberg JJ (2002) A finite element model of cell deformation during magnetic bead twisting. *J Appl Physiol* 93:1429–1436.
22. Roos KP, Brady AJ (1990) Osmotic compression and stiffness changes in relaxed skinned cardiac myocytes in PVP-40 and dextran T-500. *Biophys J* 58:1273–1283.
23. Steltenkamp S, Rommel C, Wegener J, Janshoff A Membrane stiffness of animal cells challenged by osmotic stress. *Small* 2(8–9):1016–1020, 2006.
24. An SS, Fabry B, Trepat X, Wang N, Fredberg JJ (2006) Do biophysical properties of the airway smooth muscle in culture predict airway hyperresponsiveness? *Am J Respir cell Mol Biol* 35:55–64.
25. Hoffman BD, Massiera G, Van Citters KM, Crocker JC (2006) The consensus mechanics of cultured mammalian cells. *Proc Natl Acad Sci USA* 103:10259–10264 .
26. An SS, et al. (2004) Role of heat shock protein 27 in cytoskeletal remodeling of the airway smooth muscle cell. *J Appl Physiol* 96:1701–1713.
27. Bursac P, et al. (2007) Cytoskeleton dynamics: Fluctuations within the network. *Biochem Biophys Res Comm* 355:324–330.
28. Fernandez P, Pullarkat PA, Ott A (2006) A master relation defines the nonlinear viscoelasticity of single fibroblasts. *Biophys J* 90:3796–3805.
29. Angell CA (1995) Formation of glasses from liquids and biopolymers. *Science* 267:1924–1935.
30. Kulicke WM, Porter RS (1980) Relation between steady shear flow and dynamic rheology. *Rheol Acta* 19:601–605.
31. Fabry B, et al. (2003) Time scale and other invariants of integrative mechanical behavior in living cells. *Phys Rev* 68(4 Pt 1):041914.
32. Lenormand G, Millet E, Fabry B, Butler J, Fredberg J (2004) Linearity and time-scale invariance of the creep function in living cells. *J Roy Soc Interface* 1:91–97.
33. Sollich P (1998) Rheological constitutive equation for a model of soft glassy materials. *Phys Rev E* 58:738–759.
34. Mooney M (1951) The viscosity of a concentrated suspension of spherical particles. *J Colloid Sci* 6:162–170.
35. Shen T, Wolynes PG (2005) Nonequilibrium statistical mechanical models for cytoskeletal assembly: Towards understanding tensegrity in cells. *Phys Rev E* 72:041927.
36. Chong SH, Gotze W, Singh AP (2000) Mode-coupling theory for the glassy dynamics of a diatomic probe molecule immersed in a simple liquid. *Phys Rev E* 63:011206.
37. Homouz D, Perham M, Samiotakis A, Cheung MS, Wittung-Stafshede P (2008) Crowded, cell-like environment induces shape changes in aspherical protein. *Proc Natl Acad Sci USA* 105:11754–11759.
38. Roovers J (1994) Concentration dependence of the relative viscosity of star polymers. *Macromolecules* 27:5359–5364.
39. Buitenhuis J, Forster S (1997) Block copolymer micelles: Viscoelasticity and interaction potential of soft spheres. *J Chem Phys* 107:262–272.
40. Kobelev V, Schweizer KS (February 2, 2005) Strain softening, yielding, and shear thinning in glassy colloidal suspensions. *Phys Rev E*, 10.1103/PhysRevE.71.021401.
41. Xia X, Wolynes PG (2000) Fragilities of liquids predicted from the random first order transition theory of glasses. *Proc Natl Acad Sci USA* 97:2990–2994.
42. Lubchenko V, Wolynes PG (2007) Theory of structural glasses and supercooled liquids. *Ann Rev Phys Chem* 58:235–266.